MATHEMATICAL MODELING AND COMPUTING, Vol. 12, No. 2, pp. 540–548 (2025)

Quantum antibunching in nonlinear couplers: a phase space approach using the positive P-representation

Hanapi M. S. M.[1], Ibrahim A.-B. M. A.[1,*], Julius R.[2], Choudhury P. K.[3]

[1] *Faculty of Applied Sciences, University Teknologi MARA (UiTM), 40450 Shah Alam, Selangor, Malaysia*
[2] *Faculty of Applied Sciences, University Teknologi MARA (UiTM) Perak, Tapah Campus, Perak, Malaysia*
[3] *International Research Center for Advanced Photonics, Zhejiang University, Building 1A, 718 East Haizhou Rd., Haining Zhejiang 314400, P.R. China*
[*] *Corresponding author: abdelbaset@uitm.edu.my*

(Received 7 January 2025; Revised 1 June 2025; Accepted 2 June 2025)

Quantum antibunching, vital for single-photon sources, enables applications in quantum technology, such as secure communication and quantum computing. This study investigates photon antibunching generation in a Nonlinear coupler (NLC) comprising two coupled waveguides: one linear and one with the second-order nonlinearity. Each waveguide is excited by a coherent laser source, with the second harmonic generation enhancing antibunching. Using the Schrödinger picture, the system's Hamiltonian is transformed into a master equation via the Liouville–von Neumann equation. The master equation is further translated into a Fokker–Planck equation using the positive-P representation and subsequently mapped to stochastic differential equations via Ito rules for numerical analysis. The effects of input parameters on antibunching behavior are examined, showcasing the potential of simple systems like NLCs for precise single-photon manipulation, advancing quantum technology.

Keywords: *quantum optics; nonlinear coupler; positive P-representation; photon antibunching.*

2010 MSC: 81V80, 81Q05, 60H10, 78A60 **DOI:** 10.23939/mmc2025.02.540

1. Introduction

Moore's Law predicts the number of transistors on a microchip doubles approximately every two years, thereby leading to an exponential increase in computational power and a decrease in relative cost. This has driven the rapid advancement in classical electronics technology for several decades [1]. However, as silicon-based transistors reach the physical and economic limits at atomic scales, quantum effects such as tunneling and superposition, along with heat dissipation, interfere with the operation of classical transistors, making further miniaturization impractical. Quantum technology, however, offers a promising alternative, capable of solving complex problems more efficiently and potentially overcoming the constraints faced by silicon-based transistors. It utilizes the principles of quantum mechanics to perform tasks beyond the capability of classical technology. Quantum data is represented by qubits with unique properties that allow quantum computers to solve complex problems significantly faster than classical computers [2]. Additionally, it offers advanced security algorithms, making certain types of hacking computationally impossible [3]. Achieving these advancements relies on the unique behavior of quantum particles. Consequently, obtaining photons with quantum properties is essential for the progress of quantum technology.

Photon antibunching is a quantum phenomenon where photons are emitted one at a time, rather than in bunches — a behavior distinct from classical light sources, where photons can be emitted in groups. In an antibunched light source, the probability of detecting two photons simultaneously (or within a very short time interval) is significantly reduced. This results in photons being uniformly

spaced over time. Unlike photons from classical light, antibunched photons are uniformly spaced in their trajectory and are rarely detected close together in time. This behavior is a hallmark of single-photon sources [4,5], which are essential components in various quantum technologies, including quantum cryptography and quantum computing [6]. Initially, the Hanbury Brown and Twiss (HBT) experiment observed that photons tend to arrive in bunches for classical light sources [7]. Later, photon antibunching was experimentally observed by Kimble, Dagenais, and Mandel [8]. They found that the probability of detecting two photons simultaneously was significantly reduced, thereby verifying the phenomenon of photon antibunching. Subsequently, photon antibunching has been extensively studied, and various mechanisms have been proposed to achieve antibunching effects. These include vacuum-induced coupling (VIC) [9], the utilization of Kerr nonlinearity in two-cavity systems [10], and the investigation of non-degenerate parametric oscillators [11].

An optical coupler is a device comprising two or more closely positioned waveguides, typically optical fibers, which allow light to be transferred between them due to being in proximity. In a Nonlinear coupler (NLC), at least one of the waveguides comprises a material that exhibits a nonlinear optical response, such as the second or third-order nonlinearity. This significantly influences the light propagation dynamics, enabling the coupler to exhibit a range of unique behaviors that are not present in linear couplers. In our recent work, we proposed utilizing different versions of NLC as a source of nonclassical light, such as squeezed light [12–17] and quantum entanglement [18]. The choice of quantum NLCs as sources of nonclassical light is promising for future quantum technologies due to their design simplicity, experimental feasibility, and ease of integration with other quantum optical devices, such as quantum circuits, photonic chips, and all-optical logic gates [19, 20]. NLCs can be either symmetric (where the waveguides share similar properties) or asymmetric (with the waveguides differing in properties), such as one being linear and the other nonlinear. This asymmetry can result in distinct propagation dynamics, making it a useful design choice to achieve specific optical behaviors.

In previous studies on asymmetric NLC with the second-order nonlinearity, the analytical perturbative (AP) method has been used to approximate the quantum system dynamics [21–23]. This method is based on the Heisenberg picture, and involves deriving quantum-coupled nonlinear differential equations and solving them using the Baker–Campbell–Hausdorff (BCH) formula, truncated to the second-order commutators for computational feasibility. This truncation, while practical, inherently limits the accuracy of the AP method, particularly in systems with strong interactions. As a result, the AP method serves as a useful approximation for short evolution distances, but may not capture the full complexity of the system. In contrast, our recent work demonstrates that the positive-P representation, being a phase-space approach, provides significantly more accurate results [24, 25]. Operating within the Schrödinger picture, the positive-P method avoids the need for truncation by directly transforming the system Hamiltonian into a master equation (for the density matrix), that is converted into a classical Fokker–Planck equation (FPE). Implementing Itô calculus, the FPE is then expressed as a set of stochastic differential equations (SDEs). This approach allows for precise simulation of the system evolution, capturing quantum effects that the AP method may overlook. The ability of the positive-P method to accurately model quantum dynamics without relying on approximations makes it a more robust tool for studying nonlinear optical couplers and other complex quantum systems.

Herein, we study the possibility of generating antibunching in an asymmetrical NLC operating with the second-order nonlinearity using the positive-P representation. An asymmetrical NLC consists of two closely spaced waveguides, each supporting an optical mode from a laser source. The energy exchange between these modes occurs via coupling of the evanescent fields. The asymmetric configuration implies that one waveguide interacts linearly with its light mode, while the other interacts nonlinearly, utilizing the second-order nonlinearity. This nonlinear interaction allows for Second-Harmonic Generation (SHG), where a photon with frequency ω generates photons with double the original frequency (i.e., 2ω), thereby potentially enhancing antibunching. We analyze the impact of cross-action linear coupling between waveguides and the self-action nonlinear coupling between the field mode and the nonlinear waveguide. We also examine how the initial amplitude of the pumping modes and frequency

mismatch between the modes influence the antibunching effect. Through these investigations, we aim to uncover the underlying mechanisms governing antibunching in the system under configuration, and contribute to the design and optimization of NLC-based devices. This way, the present work aims at moving a step forward toward advancing quantum technologies by enabling precise control over single-photon generation, thereby opening up new possibilities for applications in quantum circuits, photonic chips, and other relevant quantum optical means.

2. Mathematical procedure

Phase space is a conceptual framework where every possible state of a system is represented by a unique point, defined by both the position and momentum variables [26]. In quantum optics, different representations of the quantum state, such as the Wigner, Q and positive P-representations, are used to describe quantum systems in this space. The positive P-representation, in particular, offers significant advantages over other representations by allowing a complete and non-negative probability distribution, which is essential for accurately describing quantum states, especially in systems with the strong nonlinearity [27–29]. This representation follows Schrödinger picture of quantum mechanics, where the evolution of the system is described by a time-dependent state vector while quantum operators remain constant.

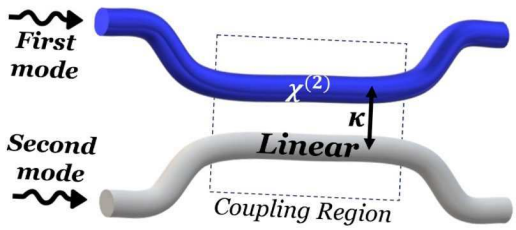

Fig. 1. Schematic diagram of two-channel asymmetric NLC, featuring a nonlinear waveguide (the first channel) and a linear waveguide (the second channel). Both waveguides are pumped with a fundamental mode; the field mode in the nonlinear waveguide is being identified as the first mode, and that in the linear waveguide as the second mode. Own sketch.

In this work, we consider the system comprising a linear and a nonlinear channel operating with SHG, as outlined in the introductory part. Figure 1 depicts the system, which can be mathematically represented by the following Hamiltonian equation:

$$\frac{\hat{H}}{\hbar} = \omega_1 \hat{a}_1^\dagger \hat{a}_1 + \omega_2 \hat{a}_2^\dagger \hat{a}_2 + \frac{ig}{2}\big(\hat{a}_1^{\dagger 2}\hat{b}_1 - \text{h.c.}\big) + 2\omega_{b_1}\hat{b}_1^\dagger \hat{b}_1 + k\big(\hat{a}_1^\dagger \hat{a}_2 + \text{h.c.}\big), \quad (1)$$

In Eq. (1), the term $\hat{a}_j^\dagger \hat{a}_j$ represents the ladder operators, where $j = 1, 2$ corresponds to the first and second fundamental modes, respectively. Also, $\hbar$ is the reduced Planck constant, ω_j is the frequency of the jth mode, g is the nonlinear coupling parameter, k is the linear coupling parameter, and "h.c." denotes the Hermitian conjugate of the preceding term. The system is driven by two fundamental modes originating from a coherent laser source, with the propagation of each mode being represented by the first two terms in Hamiltonian Eq. (1). The interaction of the first mode with a second-order nonlinear medium, leading to the SHG process, is captured by the third term $\frac{ig}{2}\big(\hat{a}_1^{\dagger 2}\hat{b}_1 - \text{h.c.}\big)$. This process generates the second harmonic mode, the propagation of which is described by the fourth term $2\omega_1 \hat{b}_1^\dagger \hat{b}_1$ of the Hamiltonian. The final term $k\big(\hat{a}_1^\dagger \hat{a}_2 + \text{h.c.}\big)$ accounts for the linear coupling between the two channels, facilitating their interaction through the exchange of evanescent fields. The time evolution of the state of a quantum system is dictated by the fundamental von Neumann equation, which governs the time evolution of the density matrix ρ of the system,

$$i\hbar \frac{d\hat{\rho}}{dt} = \big[\hat{H}, \hat{\rho}\big], \quad (2)$$

By substituting the Hamiltonian from Eq. (1) into the von Neumann Eq. (2), we obtain the following quantum master equation, which describes the time evolution of the density matrix,

$$\frac{\partial \hat{\rho}}{\partial t} = i\omega_1 \hat{\rho}\, \hat{a}_1^\dagger \hat{a}_1 + i\omega_2 \hat{\rho}\, \hat{a}_2^\dagger \hat{a}_2 + 2i\omega_1 \hat{\rho}\, \hat{b}_1^\dagger \hat{b}_1 - \frac{g}{2}\hat{\rho}\, \hat{a}_1^{\dagger 2}\hat{b}_1 + \frac{g}{2}\hat{\rho}\, \hat{a}_1^2 \hat{b}_1^\dagger + ik\hat{\rho}\, \hat{a}_1^\dagger \hat{a}_2 + ik\hat{\rho}\, \hat{a}_1 \hat{a}_2^\dagger - i\omega_1\, \hat{a}_1^\dagger \hat{a}_1 \hat{\rho} - i\omega_2\, \hat{a}_2^\dagger \hat{a}_2 \hat{\rho} - 2i\omega_1\, \hat{b}_1^\dagger \hat{b}_1 \hat{\rho} + \frac{g}{2}\, \hat{a}_1^{\dagger 2}\hat{b}_1 \hat{\rho} - \frac{g}{2}\, \hat{a}_1^2 \hat{b}_1^\dagger \hat{\rho} - ik\, \hat{a}_1^\dagger \hat{a}_2 \hat{\rho} - ik\, \hat{a}_1 \hat{a}_2^\dagger \hat{\rho}. \quad (3)$$

By applying the quantum-classical correspondence rules of the positive P-representation [27], i.e., $\hat{a}\hat{\rho} = \alpha P$, $\hat{a}^\dagger\hat{\rho} = \left(\beta - \frac{\partial}{\partial\alpha}\right)P$, $\hat{\rho}\hat{a} = \left(\alpha - \frac{\partial}{\partial\beta}\right)P$, and $\hat{\rho}\hat{a}^\dagger = \beta P$, the quantum master equation is transformed into its classical counterpart – the FPE. In this case, the quantum state of the system is represented by a quasi-probability distribution P over complex variables α and β. These variables correspond to the amplitudes of the quantum field modes. Specifically, α and α^* represent the coherent state amplitudes in one phase space, while β and β^* represent the coherent state amplitudes in an independent, yet identical, phase space. This dual phase space formulation allows for a broader range of quantum effects to be captured while maintaining a classical-like evolution in terms of stochastic differential equations. The resulting FPE is as follows:

$$\begin{aligned}\frac{\partial P}{\partial t} = \Bigg[& \frac{\partial}{\partial\alpha_1}\left(i\omega_1\alpha_1 - g\beta_1\bar{\alpha}_1 + ik\alpha_2\right) + \frac{\partial}{\partial\beta_1}\left(-i\omega_1\beta_1 - g\alpha_1\bar{\beta}_1 - ik\beta_2\right) \\ & + \frac{\partial}{\partial\alpha_2}\left(i\omega_2\alpha_2 + ik\alpha_1\right) + \frac{\partial}{\partial\beta_2}\left(-i\omega_2\beta_2 - ik\beta_1\right) \\ & + \frac{\partial}{\partial\bar{\alpha}_1}\left(2i\omega_1\bar{\alpha}_1 + \frac{g}{2}\alpha_1^2\right) + \frac{\partial}{\partial\bar{\beta}_1}\left(-2i\omega_1\bar{\beta}_1 + \frac{g}{2}\beta_1^2\right) + \frac{1}{2}\left(g\bar{\beta}_1\frac{\partial^2}{\partial\beta_1^2} + g\bar{\alpha}_1\frac{\partial^2}{\partial\alpha_1^2}\right)\Bigg] P. \end{aligned} \tag{4}$$

The first derivative terms in the above FPE represent the drift of the probability distribution, driven by deterministic forces, while the second derivative terms account for the diffusion resulting from random fluctuations. To facilitate the analysis and numerical simulation, the FPE can be transformed into a set of SDEs. This transformation is performed using Itô's lemma from stochastic calculus. The SDEs provide a more straightforward description of the stochastic dynamics of the system and are computationally more efficient to simulate. The resulting SDEs are as follows:

$$\frac{d\alpha_1}{dt} = -i\omega_1\alpha_1 + g\beta_1\bar{\alpha}_1 - ik\alpha_2 + \sqrt{g\bar{\alpha}_1}\eta_1(t), \tag{5}$$

$$\frac{d\beta_1}{dt} = i\omega_1\beta_1 + g\alpha_1\bar{\beta}_1 + ik\beta_2 + \sqrt{g\bar{\beta}_1}\eta_2(t), \tag{6}$$

$$\frac{d\alpha_2}{dt} = -i\omega_2\alpha_2 - ik\alpha_1, \tag{7}$$

$$\frac{d\beta_2}{dt} = i\omega_2\beta_2 + ik\beta_1, \tag{8}$$

$$\frac{d\bar{\alpha}_1}{dt} = -2i\omega_1\bar{\alpha}_1 - \frac{g}{2}{\alpha_1}^2, \tag{9}$$

$$\frac{d\bar{\beta}_1}{dt} = 2i\omega_1\bar{\beta}_1 - \frac{g}{2}{\beta_1}^2. \tag{10}$$

In Eqs. (5) and (6), $\eta_j(t)$ represents random fluctuations arising from the diffusion term in the FPE. For stability in numerical simulations, it is more convenient to scale the SDEs system Eqs. (5)–(10) into a dimensionless form. This is accomplished by scaling both sides with respect to the input frequency ω_1 of the first mode, leading to the dimensionless parameters

$$\widetilde{\omega}_1 = \frac{\omega_1}{\omega_1} = 1, \quad \widetilde{g} = g\omega_1, \quad \widetilde{k} = \frac{k}{\omega_1}, \quad \widetilde{\eta}_j(\tau) = \frac{\eta_j(t)}{\sqrt{\omega_1}}, \quad \tau = \omega_1 t. \tag{11}$$

Hence, we have a new set of dimensionless parameters $\widetilde{\omega}_1$, $\widetilde{g}$, $\widetilde{k}$, $\widetilde{\eta}_j$, and τ, corresponding to the dimensional parameters ω_1, g, k, η_j, and t, respectively. The solution of the SDEs system (5)–(10) over many trajectories is then computed to produce the complex variables α_1, β_1, α_2, β_2, $\bar{\alpha}_1$, and $\bar{\beta}_1$, which will subsequently be used to assess the possibility of antibunching. Antibunching can be assessed using the expression of the correlation function [23];

$$D_j = \langle\hat{N}_j^2\rangle - \langle\hat{N}_j\rangle^2 - \langle\hat{N}_j\rangle, \tag{12}$$

where $N_j = a_j^\dagger a_j$ represents the average photon number in the jth mode. When $D_j = 0$, this corresponds to a coherent state where the photon statistics are Poissonian, while $D_j > 0$ and $D_j < 0$

correspond to photon bunching and antibunching, respectively. In the positive P-representation, operators must be in normal order, meaning that in any product of creation and annihilation operators, all creation operators are positioned to the left of all annihilation operators. For the normal ordering of the correlation function D_j, it is expressed in terms of the creation and annihilation operators, as follows:

$$D_j = \langle \hat{a}_j^\dagger \hat{a}_j^\dagger \hat{a}_j \hat{a}_j \rangle - \langle \hat{a}_j^\dagger \hat{a}_j \rangle^2. \tag{13}$$

The correlation function is expressed in terms of the positive P complex phase space variables as

$$D_j = \langle \beta_j^2 \alpha_j^2 \rangle - \langle \beta_j \alpha_j \rangle^2, \tag{14}$$

where the subscript j represents the mode number. The scaled system of SDEs (5)–(10) is solved using the 4$^{\text{th}}$-order Runge–Kutta method over multiple trajectories to compute the complex variables α_i and β_j, which are then substituted into Eq. (14) to examine the possibility of antibunching.

3. Results and discussion

Figure 2 illustrates the results when both waveguides (in Figure 1) are pumped with two field modes of different initial amplitudes, i.e., $\alpha_1 \neq \alpha_2$. Specifically, the mode in the first (nonlinear) waveguide is fixed at $\alpha_1 = 1$, whereas the initial amplitude of the second mode in the linear waveguide is gradually increased, considering α_2 to be 0.1, 0.5, and 0.8. When the curve oscillates above the $D_1 = 0$ line, it indicates photon bunching. In this regime, photons tend to arrive in groups rather than individually, leading to a higher probability of detecting multiple photons simultaneously compared to a coherent state. Conversely, when the curve dips below the $D_1 = 0$ line, it signifies photon antibunching, where photons are more likely to be spaced apart in time, thereby reducing the likelihood of simultaneous photon detection. The oscillations in the curve represent the dynamic interplay between the bunching and antibunching as the system evolves in time (τ). The increasingly pronounced antibunching (indicated by deeper dips below the $D_1 = 0$ line) with increasing initial amplitude of the second mode suggests that the quantum nature of light, such as the single-photon characteristics, becomes more prominent when the amplitudes of the two modes are closer in magnitude.

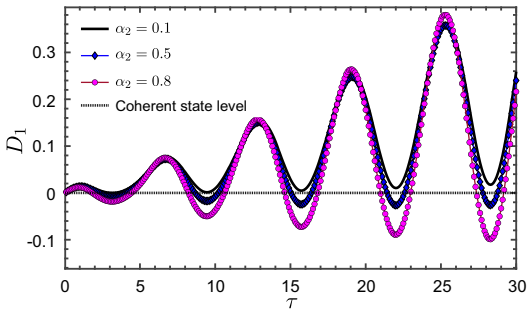

Fig. 2. The correlation function for the nonlinear waveguide mode D_1 (the first mode) as a function of scaled time τ. The amplitude of the first mode is fixed at $\alpha_1 = 1$, whereas that of the second mode in the linear waveguide is gradually increased. The other input parameters are $\widetilde{\omega}_1 = \widetilde{\omega}_2 = 1$, $\widetilde{g} = 0.01$, and $\widetilde{k} = 0.5$.

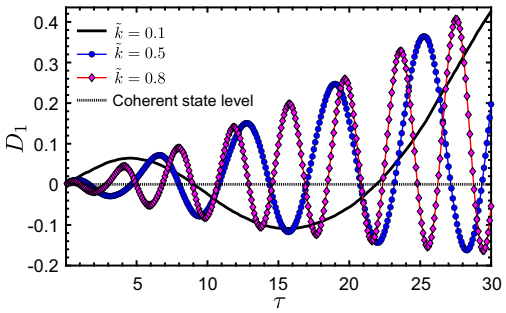

Fig. 3. The correlation function for the nonlinear waveguide mode (the first mode) as a function of scaled time τ at different values of the linear coupling coefficient $\widetilde{k}$. The other input parameters are $\alpha_1 = \alpha_2 = 1$, $\widetilde{\omega}_1 = \widetilde{\omega}_2 = 1$, and $\widetilde{g} = 0.01$.

Figure 3 illustrates the antibunching behavior of the system as a function of the linear coupling parameter $\widetilde{k}$, which governs the rate of energy transfer between the two channels via the evanescent field coupling. Increasing $\widetilde{k}$ corresponds to a reduction in the separation between the waveguides, thereby enhancing the coupling strength. Unlike the results shown in Figure 2, the data in this figure are generated under conditions of symmetrical amplitude initialization, where both modes are initially set to the same amplitude, i.e., $\alpha_1 = \alpha_2 = 1$. At a low coupling parameter $\widetilde{k} = 0.1$, the system exhibits slow oscillations, indicating a gradual exchange of energy between the channels. However, as the coupling parameter increases to $\widetilde{k} = 0.5$ and/or $\widetilde{k} = 0.8$, the oscillations become more rapid and

pronounced. This oscillatory behavior is likely due to the increased rate of energy transfer between the waveguides as they are brought closer. Faster oscillations reflect a more dynamic interaction between the two modes, with the energy being exchanged more quickly as the coupling strength increases. It should be noted that the cases for linear coupling parameters $\widetilde{k} = 0.2$ and $\widetilde{k} = 0.3$ are not shown in Figure 3, but the trend remains the same: as $\widetilde{k}$ increases, the oscillations speed up, indicating faster energy exchange between the waveguides, similar to what is observed for $\widetilde{k} = 0.5$ and/or $\widetilde{k} = 0.8$.

Amplifying the nonlinear coupling parameter, which reflects the strength of nonlinear interactions, leads to a marked reduction in the duration of antibunching. As Figure 4 shows, where $\widetilde{g} = 0.03$, the antibunching diminishes more quickly compared to $\widetilde{g} = 0.01$. Furthermore, a faster reduction in the antibunching period is observed at $\widetilde{g} = 0.05$. These results highlight the drawbacks of employing strong nonlinear interactions, i.e., while they amplify antibunching effects at early evolution stages, they do so over a much shorter time span. This indicates that excessively strong nonlinear coupling may not be ideal for sustaining antibunching over longer periods, thereby limiting its practical application.

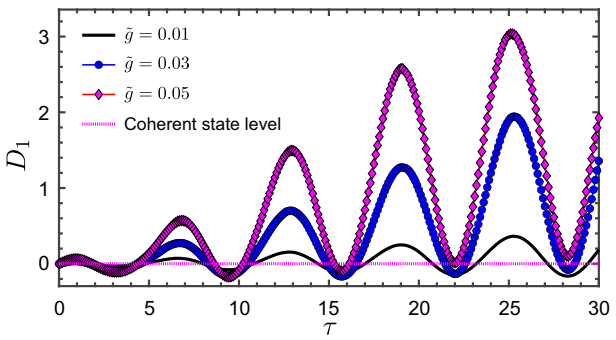

Fig. 4. The correlation function for the nonlinear waveguide mode (the first mode) as a function of scaled time at different values of nonlinear coupling coefficient $\widetilde{g}$. The other input parameters are $\alpha_1 = \alpha_2 = 1$, $\widetilde{\omega}_1 = \widetilde{\omega}_2 = 1$, and $\widetilde{k} = 0.5$.

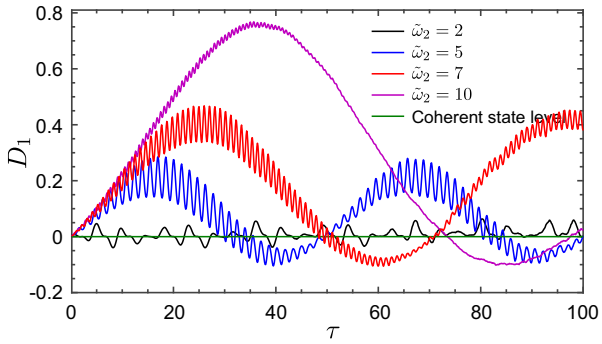

Fig. 5. Antibunching in the first pump mode for $\widetilde{\omega}_2 = 2$, $\widetilde{\omega}_2 = 5$, and $\widetilde{\omega}_2 = 7$. The other input parameters are $\alpha_1 = \alpha_2 = 1$, $\widetilde{\omega}_1 = 1$, $\widetilde{g} = 0.01$, and $\widetilde{k} = 0.5$.

Figure 5 depicts the antibunching curves for various degrees of frequency mismatch, achieved by varying the frequency $\widetilde{\omega}_2$ of the second mode, while maintaining the frequency of the first mode constant at $\widetilde{\omega}_1 = 1$. The results highlight how the degree of frequency mismatch influences the temporal evolution of the antibunching parameter D_1 in the nonlinear waveguide. In the case of slight frequency mismatch with $\widetilde{\omega}_2 = 2$, the antibunching dynamics exhibit small, irregular oscillations that suggest a more chaotic and unpredictable system behavior. This indicates that the quantum interference effects of the system are more complex, possibly due to the near-resonance condition that induces a more intricate interplay between the modes. A gradual change in the irregular oscillations is observed when $\widetilde{\omega}_2$ is set to 3 or 4. As the frequency mismatch increases to these values, the oscillations in D_1 begin to smooth out, indicating a transition to more stable behavior. However, for clarity, these cases were not shown in Figure 5. As the frequency mismatch increases to $\widetilde{\omega}_2 = 5$ and $\widetilde{\omega}_2 = 7$, the oscillations in D_1 become more regular and predictable, reflecting a relatively stabilized quantum state dynamics. The evolution shows well-defined oscillatory patterns, with clearer distinctions between bunching and antibunching regions. This indicates that increasing the frequency mismatch reduces the complexity of mode interactions, allowing the system to settle into more stable quantum states. However, with a significant frequency mismatch (with $\widetilde{\omega}_2 = 10$), while the oscillations remain regular, the onset of antibunching (i.e., the negative values of D_1) is delayed, occurring at a later time τ. This delay indicates that a stronger frequency mismatch initially suppresses the quantum interference effects necessary for antibunching, likely because the modes are too detuned to interact effectively at early times. Over time, as the system evolves, the interactions still lead to antibunching, but the delayed response suggests that higher mismatches make it more challenging to achieve and maintain antibunching.

Overall, while increasing frequency mismatch can lead to more predictable antibunching behavior, it also delays the onset of antibunching, especially at higher mismatches. This offers valuable insight into the balance required between frequency matching and mismatch in designing systems for controlled quantum light generation.

4. Conclusion

It can be concluded from the above results that, compared to the Heisenberg-based AP method, the positive P-approach offers relatively higher accuracy in simulating the complex quantum interactions within the coupler, providing a more reliable analysis of the quantum states of the system. The findings reveal that the linear and nonlinear coupling strengths, along with frequency mismatches, play critical roles in shaping the antibunching characteristics. Specifically, increasing the linear coupling parameter intensifies the oscillatory behavior of antibunching, leading to rapid fluctuations. On the other hand, stronger nonlinear coupling enhances the peak amplitude of antibunching but shortens its duration. Additionally, frequency mismatch has significant impact on the system behavior. In particular, a slight mismatch can induce chaotic fluctuations, while a large mismatch delays the onset of antibunching. An important observation is that significant amount of antibunching is achieved only under symmetrical amplitude initialization. This demonstrates the necessity for careful parameter tuning in designing devices for controlled quantum light generation. Overall, this work highlights the potential of simple, yet highly effective, NLCs for advancing quantum technology by providing precise control over single-photon generation. Future experimental validation will be essential to confirm these theoretical predictions and to pave the way for practical implementations in quantum communication and computing applications.

Acknowledgements

A.-B. M. A. Ibrahim acknowledges the financial support by the Ministry of Higher Education (MOHE, Malaysia) through the grant FRGS/1/2021/STG07/UITM/02/10.

[1] Mack C. A. Fifty years of Moore's law. IEEE Transactions on Semiconductor Manufacturing. **24** (2), 202–207 (2011).

[2] Li H., Zhao G. The Comparison of the computing ability of quantum and conventional computer. Highlights in Science, Engineering and Technology. **5**, 68–74 (2022).

[3] Akter M. S., Rodriguez-Cardenas J., Shahriar H., Cuzzocrea A., Wu F. Quantum cryptography for enhanced network security: A comprehensive survey of research, developments, and future directions. 2023 IEEE International Conference on Big Data (BigData). 5408–5417 (2023).

[4] Jiang Q., Roy P., Claude J.-B., Wenger J. Single photon source from a nanoantenna-trapped single quantum dot. Nano Letters. **21** (16), 7030–7036 (2021).

[5] Ren Y., Duan Z., Fan B., Guan S., Xie M., Liu C. Antibunched single-photon/photon-pair emission with coupled Jaynes-Cummings model. Optics Express. **30** (12), 21787–21796 (2022).

[6] Santori C., Fattal D., Yamamoto Y. Single-photon devices and applications. John Wiley & Sons (2010).

[7] Brown H. R., Twiss R. Q. A test of a new type of stellar interferometer on Sirius. A Source Book in Astronomy and Astrophysics, 1900–1975. Harvard University Press, 8–12 (1979).

[8] Kimble H. J., Dagenais M., Mandel L. Photon antibunching in resonance fluorescence. Physical Review Letters. **39** (11), 691 (1977).

[9] Wu Z., Li J., Wu Y. Vacuum-induced quantum-beat-enabled photon antibunching. Physical Review A. **108** (2), 023727 (2023).

[10] Zhu H., Li X., Li Z., Wang F., Zhong X. Strong antibunching effect under the combination of conventional and unconventional photon blockade. Optics Express. **31** (13), 22030–22039 (2023).

[11] Mandal S., Alam M., Kora M., Wahiddin M. R. Antibunching of photons in a coherent radiation field coupled to a non-degenerate parametric oscillator beyond rotating wave approximation. Pramana. **95**, 82 (2021).

[12] Julius R., Ibrahim A.-B. M. A., Deni M. S. Quantum state generation in a four-mode Kerr nonlinear directional coupler. Laser Physics. **24** (3), 035202 (2014).

[13] Julius R., Ibrahim A.-B. M. A., Choudhury P. K., Eleuch H. On the nonclassical dynamics of cavity-assisted four-channel nonlinear coupler. Chinese Physics B. **27** (11), 114206 (2018).

[14] Julius R., Ibrahim A.-B. M. A., Abd-Rahman M. K., Choudhury P. K. Quantum dynamics of a four-channel Kerr nonlinear directional coupler. Optical Review. **25** (5), 563–570 (2018).

[15] Julius R., Ibrahim A.-B. M. A., Choudhury P. K., Eleuch H. Quantum states generation in multichannel directional coupler with second-order nonlinearity. Optik. **186**, 212–220 (2019).

[16] Julius R., Ibrahim A.-B. M. A., Eleuch H., Choudhury P. K. Sub-Poissonian photon squeezing and entanglement in optical chain second harmonic generation. Journal of Modern Optics. **66** (10), 1129–1138 (2019).

[17] Julius R., Zahirzai M., Ibrahim A.-B. M. A., Eleuch H., Choudhury P. K. Single-and compound-mode squeezing in nonlinear coupler with frequency mismatch. Journal of Electromagnetic Waves and Applications. **34** (3), 301–315 (2020).

[18] Hanapi M. S. M., Ibrahim A.-B. M. A., Choudhury P. K. On the perturbative approach to analyse entanglement in two-channel Kerr nonlinear coupler. Optik. **243**, 167420 (2021).

[19] Zhang Y., McKnight L., Engin E., Watson I. M., Cryan M. J., Gu E., Thompson M. G., Calvez S., O'Brien J. L., Dawson M. D. GaN directional couplers for integrated quantum photonics. Applied Physics Letters. **99**, 161119 (2011).

[20] Li H. W., Przeslak S., Niskanen A. O., Matthews J. C. F., Politi A., Shadbolt P., Laing A., Lobino M., Thompson M. G., O'Brien J. L. Reconfigurable controlled two-qubit operation on a quantum photonic chip. New Journal of Physics. **13** (11), 115009 (2011).

[21] Mandal S., Perina J. Approximate quantum statistical properties of a nonlinear optical coupler. Physics Letters A. **328** (2–3), 144–156 (2004).

[22] Thapliyal K., Pathak A., Sen B., Peřina J. Higher-order nonclassicalities in a codirectional nonlinear optical coupler: Quantum entanglement, squeezing, and antibunching. Physical Review A. **90** (1), 013808 (2014).

[23] Thapliyal K., Pathak A., Sen B., Perina J. Nonclassical properties of a contradirectional nonlinear optical coupler. Physics Letters A. **378** (46), 3431–3440 (2014).

[24] Hanapi M. S. M., Ibrahim A. B. M. A., Julius R., Eleuch H. Quantum Kerr nonlinear coupler: analytical versus phase-space method. Canadian Journal of Physics. **99** (9), 832–840 (2021).

[25] Hanapi M. S. M., Ibrahim A.-B. M. A., Julius R., Choudhury P. K., Eleuch H. Nonclassical light in a three-waveguide coupler with second-order nonlinearity. EPJ Quantum Technology. **11**, 51 (2024).

[26] Schleich W. P. Quantum optics in phase space. John Wiley & Sons (2015).

[27] Drummond P. D., Gardiner C. W. Generalised P-representations in quantum optics. Journal of Physics A: Mathematical and General. **13** (7), 2353 (1980).

[28] Schack R., Schenzle A. Positive P representation. Physical Review A. **44** (1), 682 (1991).

[29] Gilchrist A., Gardiner C. W., Drummond P. D. Positive P representation: Application and validity. Physical Review A. **55** (4), 3014 (1997).

Квантове антигрупування в нелінійних спрямовувачах: підхід фазового простору з використанням позитивного P-представлення

Ханапі М. С. М.[1], Ібрагім А.-Б. М. А.[1], Юліус Р.[2], Чоудхурі П. К.[3]

[1] *Факультет прикладних наук, Університет Технології MARA (UiTM), 40450 Шах-Алам, Селангор, Малайзія*
[2] *Факультет прикладних наук, Університет Технології MARA (UiTM) Перак, Кампус Тапах, Перак, Малайзія*
[3] *Міжнародний науково-дослідний центр передової фотоніки, Чжецзянський університет, буд. 1A, 718 Ist Хейчжоу Роуд, Хайнін Чжецзян 314400, КНР*

Квантове антигрупування, життєво важливе для джерел поодиноких фотонів, відкриває можливості для застосувань у квантових технологіях, таких як безпечний зв'язок і квантові обчислення. Це дослідження вивчає генерацію антигрупування фотонів у нелінійному спрямовувачі (NLC), що складається з двох зв'язаних хвилеводів: одного лінійного та одного з нелінійністю другого порядку. Кожен хвилевід збуджується когерентним лазерним джерелом, причому генерація другої гармоніки посилює антигрупування. Використовуючи картину Шредінгера, гамільтоніан системи перетворюється на головне рівняння за допомогою рівняння Ліувілля–фон Неймана. Головне рівняння далі перетворюється на рівняння Фоккера–Планка за допомогою позитивного P-представлення та згодом відображається на стохастичні диференціальні рівняння за допомогою правил Ito для чисельного аналізу. Досліджено вплив вхідних параметрів на поведінку антигрупування, демонструючи потенціал простих систем, таких як NLC, для точної маніпуляції одинокими фотонами, сприяючи розвитку квантових технологій.

Ключові слова: *квантова оптика; нелінійний спрямовувач; позитивне P-представлення; антигрупування фотонів.*